Supplementary Information for "Prolonged $^{187}Os/^{188}Os$ excursion implies hydrothermal influence after the Chicxulub impact in the Gulf of Mexico"

Honami Sato[1,2]*, Akira Ishikawa[3,2], Ignacio Arenillas[4], José A. Arz[4], Vicente Gilabert[4,5], Philippe Claeys[6], Steven Goderis[6], Christopher M. Lowery[7], Sean P.S. Gulick[7,8,9], Joanna V. Morgan[10]

[1]Department of Earth and Planetary Sciences, Kyushu University, Fukuoka, 819-0395, Japan.
[2]Submarine Resources Research Center, Research Institute for Marine Resources Utilization, Japan Agency for Marine-Earth Science and Technology, Yokosuka, Kanagawa, 237-0061, Japan.
[3]Department of Earth and Planetary Sciences, Institute of Science Tokyo, Meguro-ku, Tokyo, 152-8550, Japan.
[4]Departamento de Ciencias de la Tierra, and Instituto Universitario de Investigación en Ciencias Ambientales de Aragón, Universidad de Zaragoza, E-50009 Zaragoza, Spain.
[5]Departament de Dinàmica de la Terra i de l'Oceà, Facultat de Ciències de la Terra, Universitat de Barcelona, E-08028 Barcelona, Spain.
[6]Archaeology, Environmental Changes, and Geo-Chemistry, Vrije Universiteit Brussel, BE-1050, Brussels, Belgium.
[7]Institute for Geophysics, Jackson School of Geosciences, University of Texas at Austin, Austin, TX, 78758, USA.
[8]Deparment of Geological Sciences, Jackson School of Geosciences, University of Texas at Austin, Austin, TX, 79712, USA.
[9]Center for Planetary Systems Habitability, University of Texas at Austin, Austin, TX, 79712, USA.
[10]Department of Earth Science and Engineering, Imperial College London, SW7 2AZ London, United Kingdom.

*Corresponding author. Email: sato.honami.975@m.kyushu-u.ac.jp

This file includes:

Supplementary Notes 1-2

Supplementary Figures 1-10

Supplementary References

Supplementary Note 1

Geological setting and the studied section

1. IODP-ICDP Site M0077

International Ocean Discovery Program-International Continental scientific Drilling Program (IODP-ICDP) Expedition 364 drilled Site M0077 (21°27'00" N, 89°57'00" W) located on the peak ring of the Chicxulub structure in the Yucatán Peninsula, Mexico (Fig. 1)[1]. In the upper cores, the post-impact sediments were recovered from 505.7 to 671.33 meters below seafloor (mbsf). Paleocene pelagic limestone was recovered from the base of the post-impact section (Unit 1F), which was deposited above the top of the suevite (impact breccia) interval (Unit 2A), including the transitional unit (Unit 1G; Supplementary Fig. 1). The upper peak ring interval is composed of suevite above impact melt rock from 671.33 to 747.02 mbsf. The lower peak ring interval is composed of suevite above impact melt rock from 617.33 to 747.02 mbsf. The lower peak ring interval is formed from granitoids intruded by pre-impact mafic and felsic dikes between 747.02 and 1334.69 mbsf, interspersed with suevite and impact melt rock. In this study, we focus on the early Paleocene (Danian stage) limestone (Supplementary Fig. 1). In addition, we also analyzed Re-Os isotopes and HSE concentrations for selected suevite, impact melt rocks, and granite samples for data comparison (Supplementary Fig. 2). The Biozone Dan1 (= P0) and the K/Pg dark clay bed are absent due to a small hiatus affecting the basal part of Danian (Supplementary Data 1). The first biozone identified is Dan2, characterized by the presence of *Parvularugoglobigerina longiapertura* (Supplementary Data 1).

2. Bochil section

The Bochil section (17°00'33" N, 92°56'44" W) is located in southeastern Mexico (the State of Chiapas), about 9 km northeast from the town of Bochil, along the road to the PEMEX Soyalo-1 well[2]. This section is one of the most representative K/Pg boundary outcrops in southern Mexico, containing a Chicxulub impact-linked Complex Clastic Unit (CCU), with a thickness of 86 m due to its relatively proximal position to the Chicxulub crater[3]. The CCU at Bochil consists of a fining-upward sedimentary sequence, which begins with a very thick carbonate breccia that grades to a very fine-grained sandstone and siltstone rich in ejecta (shocked mineral and accretionary lapilli horizons). The uppermost of CCU is a thin yellow-red shaly layer that represents the finest ejecta, containing the Ir anomaly and Ni-rich spinel crystals. A 6-8 cm-thick dark clay bed overlies the CCU and marks the base of the Soyaló Formation, which locally consists of marls with intercalation of marly limestones in the lowermost Danian. The lowermost centimeters of this dark clay bed belong to the Biozone Dan1 by Ref.[4] (= Biozone P0 by Ref.[5]; Supplementary Data 3), showing the continuity across the impact-linked CCU and the lowermost Paleocene (Danian) sediments composed of clay, marl, marly limestone, and limestone (Supplementary Data 3)[3]. The lowest and highest occurrences of planktic foraminiferal key-taxa occur in the correct stratigraphic order, showing its stratigraphic continuity from Dan1 to Dan4a (Supplementary Data 3)[3,4].

3. Guayal section

The Guayal section (17°32'37" N, 92°36'07" W) is located in southeastern Mexico (the State of Tabasco), about 60 km southeast of the City of Villahermosa[2]. The outcrop is one of the most representative southern Mexican K/Pg sections together with Bochil. A dark clay bed overlies the 51 m-thick CCU at this section and marks the base of the Paleocene Soyaló Formation, which locally consists of an alternation of limestones and marly limestones in the lowermost Danian. The clay bed is a 3–4 cm thick dark greenish-gray clay with interbedded reddish shales in millimeter layers. The Paleocene marly limestone is outcropped overlying the clay bed. The lowest and highest occurrences of planktic foraminiferal key-taxa occur in the correct stratigraphic order, showing its stratigraphic continuity from Dan1 to Dan4a (Supplementary Data 3) [3,4].

4. El Mulato section

The El Mulato section (24°54'01" N, 98°56'56" W) is located in northeastern Mexico (Tamaulipas State), 500 m north of El Mulato village. Between the marly Upper Cretaceous Méndez Formation and the marly Lower Paleogene Velasco Formation, there is a nearly 2 m-thick CCU that has been interpreted as the result from impact-generated tsunami currents[6]. The lower Danian is composed of marlstone overlying the CCU[7]. The

Biozone Dan1 (= P0) and the K/Pg dark clay bed are absent due to a small hiatus affecting the basal part of Danian[8]. The first biozone identified is Dan2, characterized by the presence of *Pv. longiapertura* (Supplementary Data 3).

5. La Lajilla section

The La Lajilla (23°39'48" N, 98°43'57" W) is located in northeastern Mexico (Tamaulipas State). This section is one of the few localities worldwide that contain, albeit scarcely, preserved glassy spherules linked to the K/Pg impact[6,9]. The stratigraphic sequence at La Lajilla is similar to El Mulato, but the CCU only spans 1 m (Ref.[7]). As at El Mulato, the Biozone Dan1 (= P0) and the K/Pg dark clay bed are absent due to a small hiatus affecting the basal part of Danian[4,8]. The first biozone identified unambiguously is Dan2, characterized by the presence of *Pv. longiapertura* (Supplementary Data 3). No planktic foraminiferal specimens were identified in the first Danian sample of La Lajilla (LL+0+2), so it could belong to the Biozone Dan1 (= P0) but also to the top of the CCU (Supplementary Data 3).

Supplementary Note 2

Osmium mass balance modelling across the K/Pg impact

Previous studies have shown that the Os isotopic composition of seawater is controlled by the balance between input fluxes from continental, mantle-derived and extraterrestrial sources, and is well homogenized in the global ocean because the marine residence time of Os is sufficiently longer than the timescale of the global ocean circulation[10]. To explain the observed difference in the $^{187}Os/^{188}Os_i$ recovery time after the K/Pg impact between pelagic sites (Atlantic and Southern Oceans) and the Chicxulub impact basin (Gulf of Mexico), we calculated the Os mass balance and the Os isotope mass balance in the global ocean and the Gulf of Mexico (GoM) separately using a simple two-box model (Supplementary Fig. 8).

We first established global ocean model across the K/Pg impact with the following equations[11,12]:

$$\frac{dN_{gw}}{dt} = F_{riv} + F_{man} + F_{cos} - F_{sed} + F_{impact}$$

$$\frac{N_{gw}}{7.4 + R_{gw}} \frac{dR_{gw}}{dt} = F_{riv} \frac{R_{riv} - R_{gw}}{7.4 + R_{riv}} + F_{man} \frac{R_{man} - R_{gw}}{7.4 + R_{man}} + F_{cos} \frac{R_{cos} - R_{gw}}{7.4 + R_{cos}}$$

$$-F_{sed} \frac{R_{sed} - R_{gw}}{7.4 + R_{sed}} + F_{impact} \frac{R_{impact} - R_{gw}}{7.4 + R_{impact}}$$

where *N*, *F*, and *R* represents the total molar inventory of Os in global seawater, fluxes of Os (in mol yr^{-1}), and the $^{187}Os/^{188}Os$ compositions for ocean and each flux, respectively. The subscripts gw, riv, man, cos, sed, and impact indicate global seawater, riverine, mantle, cosmic dust, sedimentary, and impact-derived Os budgets, respectively. F_{impact} is assumed to be 0 except for t = 66.001 Ma, when a large amount of meteoritic Os was abruptly added to seawater. F_{sed} is assumed to be proportional to the total mass of Os in the ocean, and can be expressed as follows:

$$F_{sed} = kN_{gw}$$

where *k* represents the proportionality factor calculated as an inverse of the residence time ($\tau = 1/k$). The parameter values used for simulating $^{187}Os/^{188}Os$ sedimentary profiles from ODP Hole 1262B (South Atlantic) and ODP Hole 690C (Maud Rise, Southern Ocean) are summarized in Supplementary Data 6. For simplicity, we assumed that pre-impact

Cretaceous seawater (1.45×10^{21} kg) has the steady-state value of $^{187}Os/^{188}Os = 0.40$, and that after the instantaneous perturbation due to the impact at 66.001 Ma, pre-impact fluxes of Os into seawater are immediately restored, while impact-derived Os is gradually removed from the ocean by burial with marine sediments. Under these assumptions, the recovery rate of seawater $^{187}Os/^{188}Os$ to pre-impact values of 0.40 is primarily controlled by the proportionality factor, i.e. the residence time, and F_{impact} has a subordinate influence[13].

We set the constant residence time $\tau = 40$ kyr, F and R for riverine, mantle, and cosmic dust Os over a time interval before and after the impact, and assume that τ, F_{cos}, R_{riv}, R_{man}, and R_{cos} are similar to those estimated for the present-day marine Os cycle[10-12,14]. In contrast, we employed significantly lower F_{riv} and higher F_{man} than the range of estimated modern values to achieve a steady-state $R_{gw} = 0.40$, the value characteristic of the latest Cretaceous and the early Paleogene. By using 1080 mol yr^{-1} as F_{riv}, which is 0.6-fold lower than the estimated modern riverine flux (= 1800 mol yr^{-1}), F_{man} was calculated to be 3304 mol yr^{-1}. These values can be attributed to lower rate of silicate weathering due to smaller continental area exposed on land and higher rate of hydrothermal activity, both of which are inferred from the higher spreading rate of sea floor relative to those for the present-day[15,16]. Although the emplacement and weathering of the Deccan Trap basalt may have played an important role in the marine Os cycle across the K/Pg boundary[17,18], we did not consider any fluctuations in continental and mantle-derived Os fluxes to the global ocean, and interpret them as contributing to the lower F_{riv} and higher F_{man} during this time interval.

To obtain the F_{impact} value, we assume that the previously estimated Os mass of 8.0×10^7 kg (= 4.21×10^8 mol), corresponding to a ~4 km diameter of chondritic impactor, was dissolved in the end-Cretaceous ocean within 1 kyr (Ref.[19]), which is significantly larger than the steady-state value of the global ocean Os inventory ($N_{gw} = 1.79 \times 10^8$ mol). This amount of unradiogenic Os input ($R_{impact} = 0.127$) provides a post-impact seawater R_{gw} down to 0.17, and takes ~200 kyr for full recovery of the Os isotope excursion to the pre-impact value, which reasonably reproduces the observed profiles (Supplementary Fig. 9).

In a second step, we constructed another box model for simulating the temporal evolution of seawater $^{187}Os/^{188}Os$ reconstructed from the Site M0077 borehole in the Chicxulub impact basin, assuming that water mass renewal in the GoM was restricted over the K/Pg interval, and Os isotopic composition of seawater in the GoM was largely controlled by the ventilation to the global ocean. Recent comprehensive data from sedimentary sections of many industrial wells distributed across the northern GoM suggest a surface water connection to the global ocean during the end of Cretaceous[20], but the level of deep-water connection may have been more restricted due to redistribution of sediments caused by the tsunami from the Chicxulub impact[7,21]. Combined with our observation that the GoM seawater at ~65.265 Ma has nearly identical $^{187}Os/^{188}Os$ to the steady-state value of global seawater before and after the impact ($^{187}Os/^{188}Os = 0.40$), we hypothesize that the renewal rate of water mass in the GoM increased with time after the impact, reaching a sufficiently high rate at ~65.265 Ma that the $^{187}Os/^{188}Os$ of the GoM and global seawater are nearly homogeneous. To evaluate this scenario, we calculate the Os mass balance and the Os isotope mass balance for the GoM using the following equations:

$$\frac{dN_{mw}}{dt} = F_{inflow} + F_{continent} + F_{meteorite} - F_{msed} - F_{outflow}$$

$$\frac{N_{mw}}{7.4 + R_{mw}} \frac{dR_{mw}}{dt} = F_{inflow} \frac{R_{inflow} - R_{mw}}{7.4 + R_{inflow}} + F_{continent} \frac{R_{continent} - R_{mw}}{7.4 + R_{continent}}$$

$$+ F_{meteorite} \frac{R_{meteorite} - R_{mw}}{7.4 + R_{meteorite}} - F_{msed} \frac{R_{msed} - R_{mw}}{7.4 + R_{msed}} - F_{outflow} \frac{R_{outflow} - R_{mw}}{7.4 + R_{outflow}}$$

where N_{mw} and R_{mw} represent the total molar inventory of Os and the $^{187}Os/^{188}Os$ composition of the seawater in the GoM, respectively. We set three Os fluxes into the GoM: inflow from the global ocean (F_{inflow}), continental input via paleo-Mississippi and other rivers ($F_{\mathrm{continent}}$), and extraterrestrial input ($F_{\mathrm{meteorite}}$) assuming that a significant quantity of meteoritic Os derived from the K/Pg impactor was supplied to the GoM seawater via erosion of impact ejecta and/or alteration of melt rocks.

It should be noted that the F_{impact} and $F_{\mathrm{meteorite}}$ are assumed to be sourced from distinct fraction of meteoritic Os: the former was transported across the globe as airborne microscopic dust and impact vapor condensates which dissolve into seawater following atmospheric settling[22]; the latter represent larger fragments of melt droplets or sheets enriched in projectile components likely distributed concentrically from the impact site[23].

Although impactites recovered from the Chicxulub structure tend to have low contributions of a projectile component, when compared to those observed in other impact structures such as Vredefort, Rochechouart, Morokweng, or in the East Clearwater Lake, presumably due to a steeply-inclined trajectory of impactor[24], we hypothesized that a protracted release of meteoritic Os from impactites could be an additional mechanism for controlling $^{187}Os/^{188}Os$ composition of the seawater in the GoM. Thus, our Os records can be used to infer changes in relative contributions of the F_{inflow} and $F_{meteorite}$ after the impact event, by assuming the constant $F_{continent}$ and negligible contributions from cosmic dust and mantle-derived fluxes.

For simplicity, $R_{continent}$, $R_{meteorite}$, and R_{inflow} are assumed to be identical to R_{riv}, R_{impact}, and R_{gw}, respectively, defined for the global ocean model, and two Os outputs from the GoM seawater, which are sedimentary flux (F_{msed}) and outflow to the global ocean ($F_{outflow}$), are assumed to preserve the $^{187}Os/^{188}Os$ composition of the contemporary seawater in the GoM (i.e., $R_{msed} = R_{outflow} = R_{mw}$). Both F_{msed} and $F_{outflow}$ can be calculated by assuming that they are proportional to the total mass of Os dissolved in the 1.45×10^{18} kg of GoM seawater, which is derived from the present-day volume of the GoM (2.4×10^6 km^3: Ref.[25]), and that the water masses of inflow and outflow are balanced.

As mentioned above, since the residence time (τ) is a critical factor for controlling the recovery rate of the $^{187}Os/^{188}Os$ perturbation, it would be possible that different τ values for the global ocean and the semi-enclosed GoM including the impact site explain their contrasting rate of $^{187}Os/^{188}Os$ recovery after the K/Pg impact. While such a difference may arise if the GoM seawater was exceptionally affected by the K/Pg extinction, the diminished particle production in the GoM surface water, presumably due to a collapse of surface water productivity or diminished export production, would reduce the removal rate of impact-derived Os dissolved in the water column (i.e. longer τ). However, recent studies of post-impact recovery of marine productivity do not lend support this hypothesis, as impact-related controls such as heterogeneous recovery related to the distance from the impact site were not detected[26–28]. Thus, we hypothesized that the surface water interaction between the GoM and the global ocean maintained their relatively homogeneous export production and common residence time of Os ($\tau = 40$ kyr).

Supplementary Fig. 9 shows one of the model profiles of $F_{meteorite}$ and the GoM renewal rate controlling F_{inflow} which provides a good fit to the measured Os recovery curve. Assuming that the two parameters changed asymptotically, the fitted curve for ~2.25 Myrs after the K/Pg impact (66.00 to 63.75 Ma) can be reproduced by the combinations that; 1) $F_{meteorite}$ decreases from 81 mol yr^{-1} to 0, and 2) the water mass renewal rate increases from 0.015 to ~0.065 Sv (=10^6 m^3 s^{-1}).

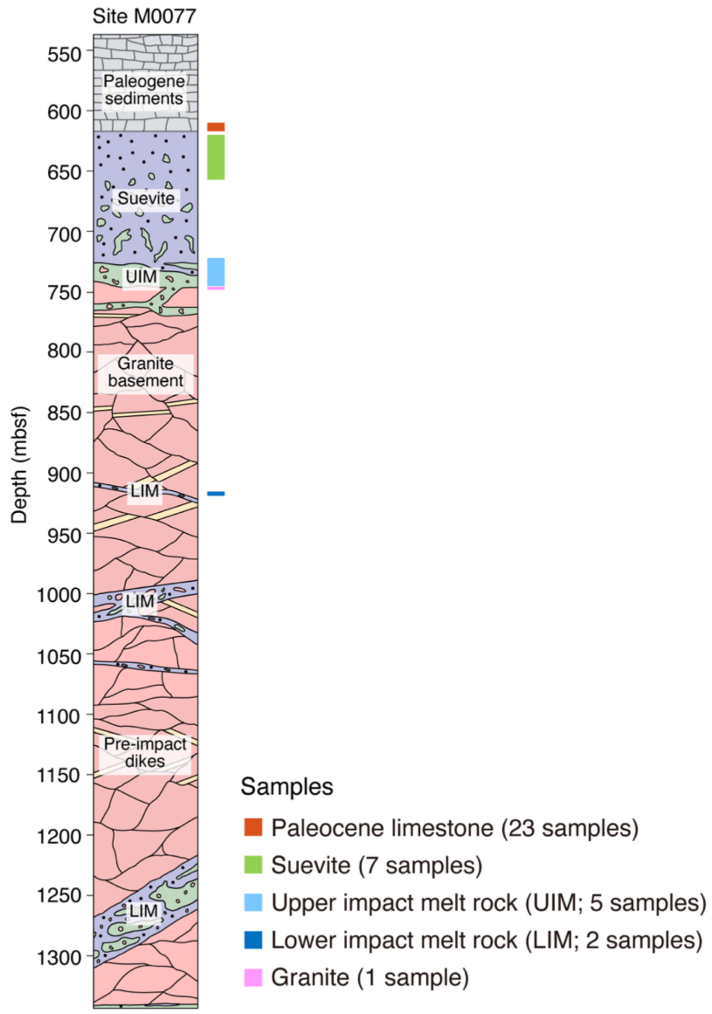

Supplementary Figure 1. Lithostratigraphy of cores drilled at Site M0077[29]. Colored bars represent sample areas for Re-Os isotope and HSE concentration analyses in this study.

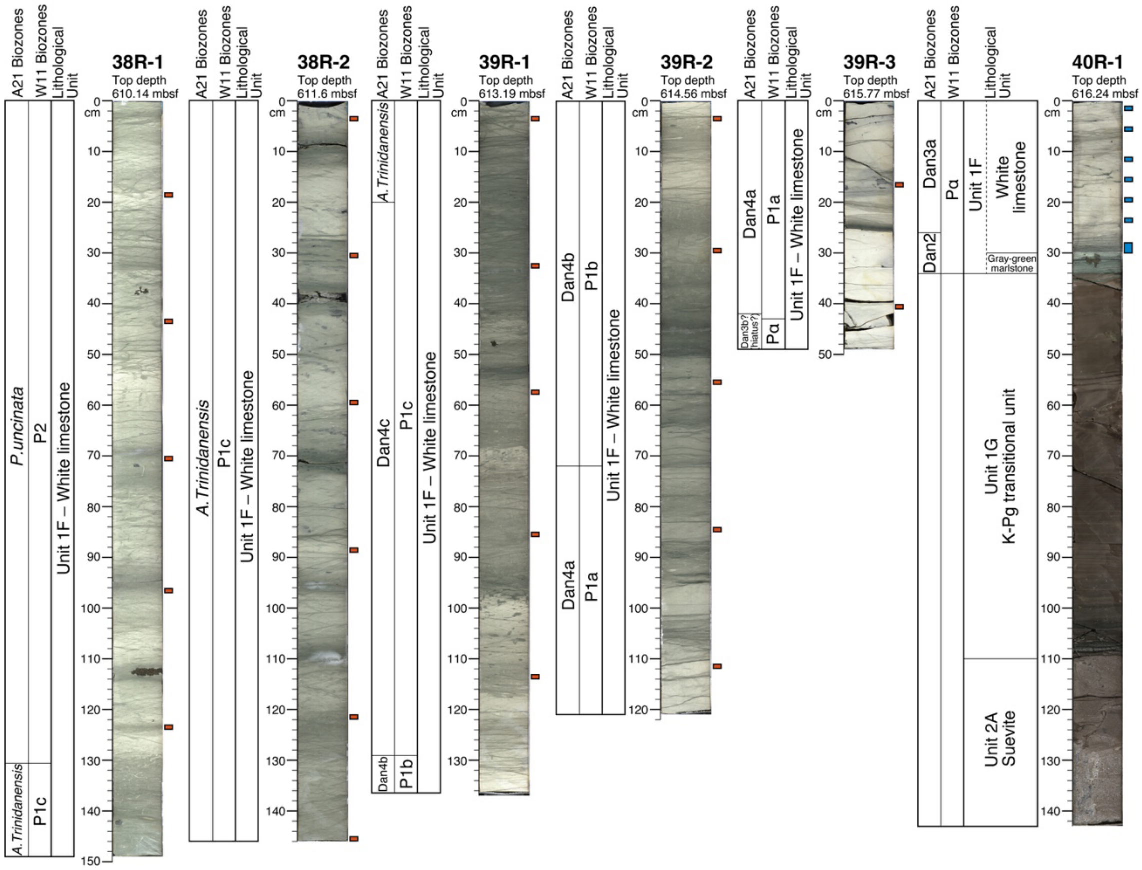

Supplementary Figure 2. Photoscan of the IODP-ICDP Expedition 364 cores 38R-1 to 40R-1 with the lithological units and new foraminiferal biozones. These core intervals, shown down-core from 610.14 to 616.67 mbsf left to right, contain suevite (Unit 2A), the transitional unit (Unit 1G), gray-green marlstone (Unit 1F), and Paleocene white limestone (Unit 1F)[1]. Sample positions in the white limestone for Re-Os isotope and HSE concentrations analyses are presented in red (this work) and blue (Ref.[22]) squares. Planktic foraminiferal biozones A21 and W11 are from Ref.[4] and Ref.[5], respectively.

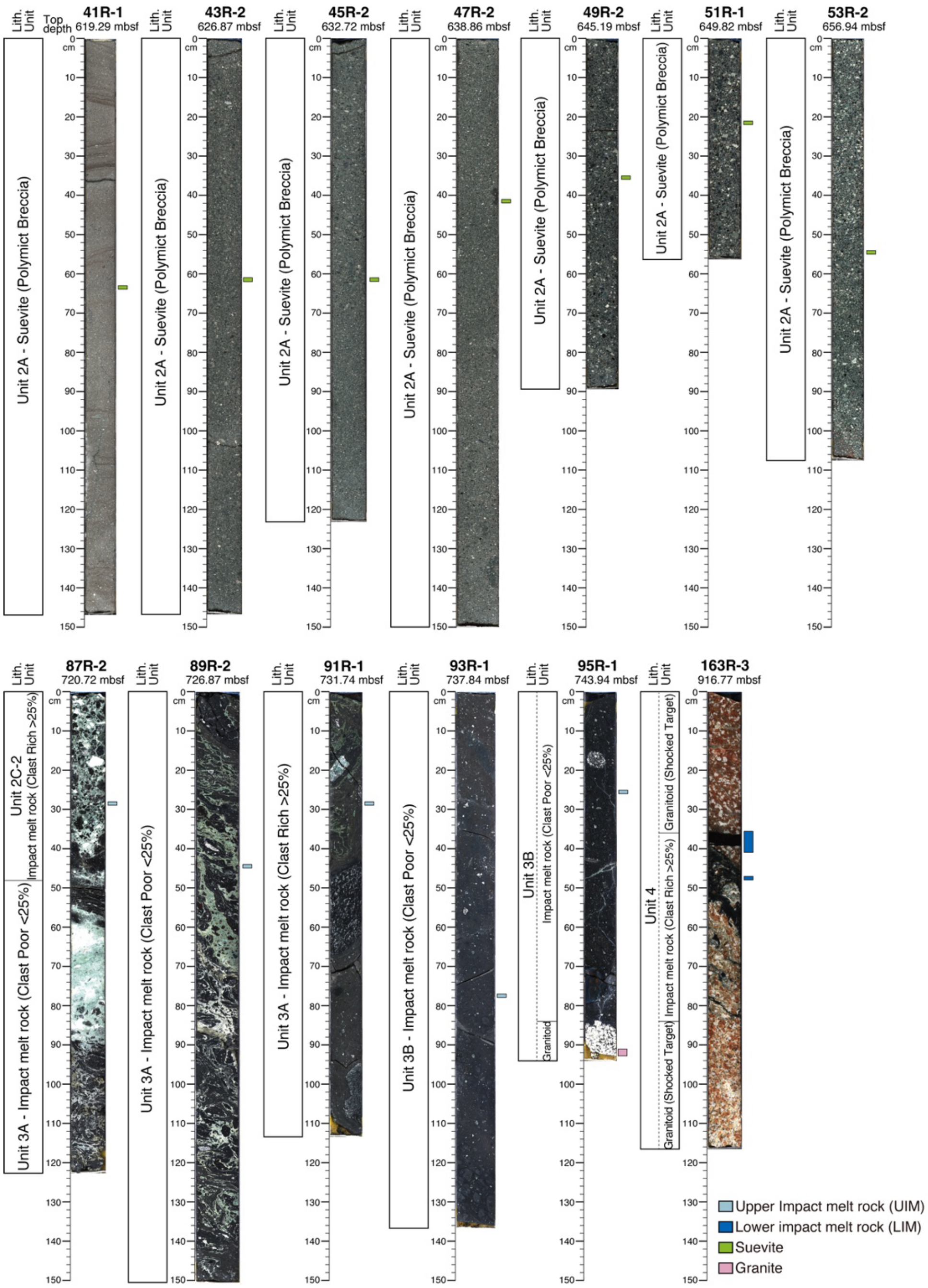

Supplementary Figure 3. Photoscan of the IODP-ICDP Expedition 364 cores 41R-1 to 163R-3 with the lithological units. These core intervals, shown down-core from 619.20 to 916.77 mbsf left to right, contain suevite, impact melt rock, and granite[1]. The lithological and textural characteristics of the upper impact melt rock (87R-2 to 95R-1) and lower impact melt rock (163R-3) are based on Refs.[30],[31]. Sample positions for Re-Os isotope and HSE concentrations analyses are presented in colored squares.

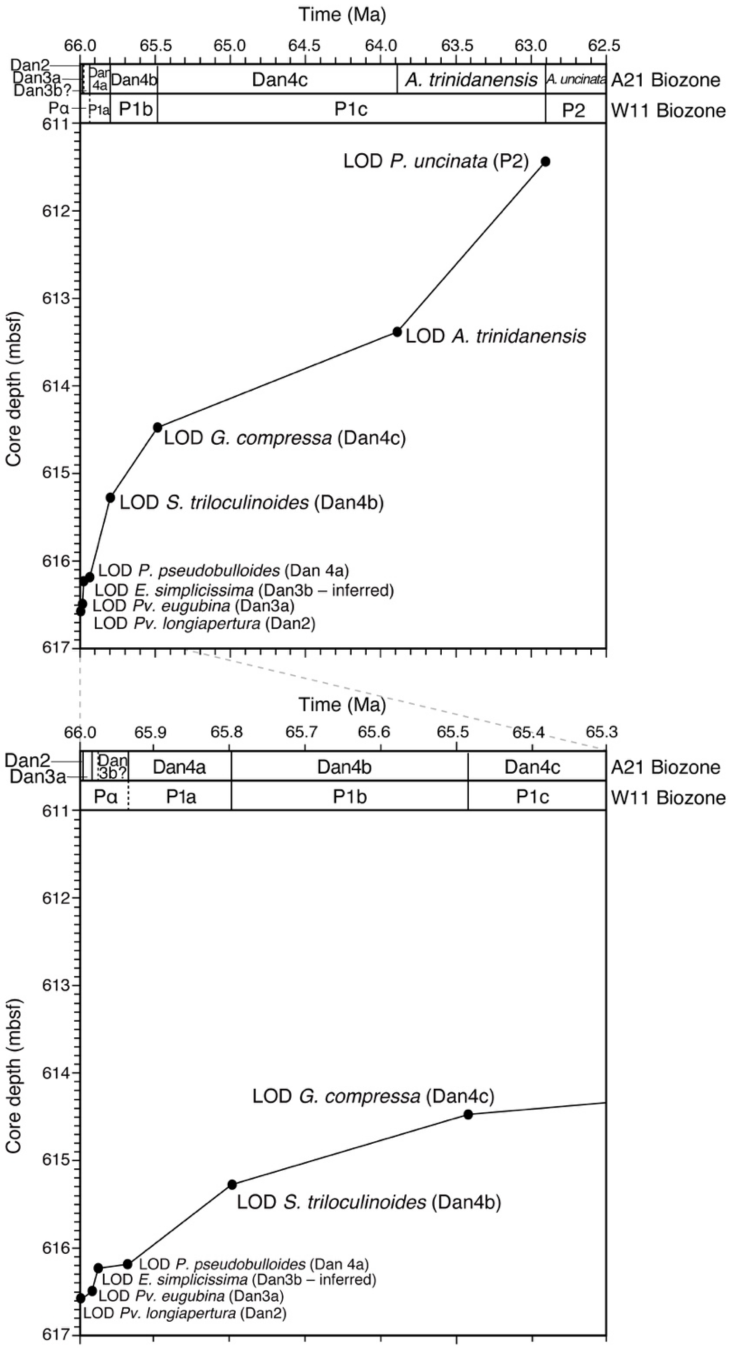

Supplementary Figure 4. Age-depth plot showing the construction of the new age model in Site M0077. Black circles are Danian planktic foraminiferal key biozonations established from Ref.[4]. The calibrated ages of stratigraphic position of key-biozones (A21) are from Ref.[4].

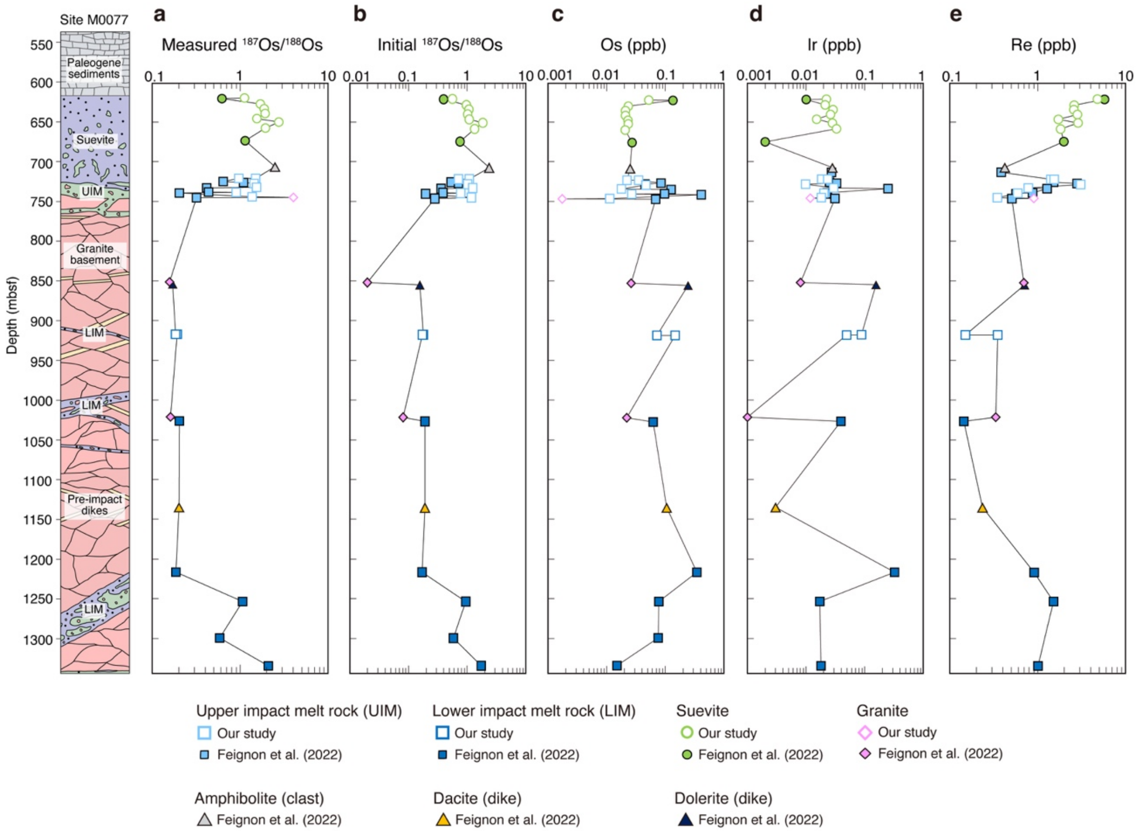

Supplementary Figure 5. Stratigraphic profile of $^{187}Os/^{188}Os$ ratios and HSE concentrations. Measured $^{187}Os/^{188}Os$ (**a**) and initial $^{187}Os/^{188}Os$ ratios ($^{187}Os/^{188}Os_i$; i = 66.001 Ma) (**b**) and Os (**c**), Ir (**d**), and Re (**e**) concentrations obtained from the suevite, impact melt rocks, and pre-impact lithologies at Site M0077[24].

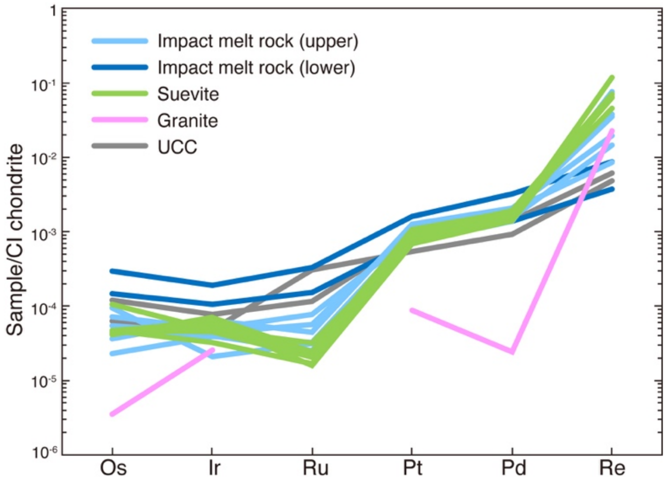

Supplementary Figure 6. CI chondrite-normalized HSE patterns of suevite, impact melt rocks, and granite at Site M0077. The HSE patterns of UCC are also shown in comparison. HSE concentrations for CI chondrite and UCC are from Refs.[32–34].

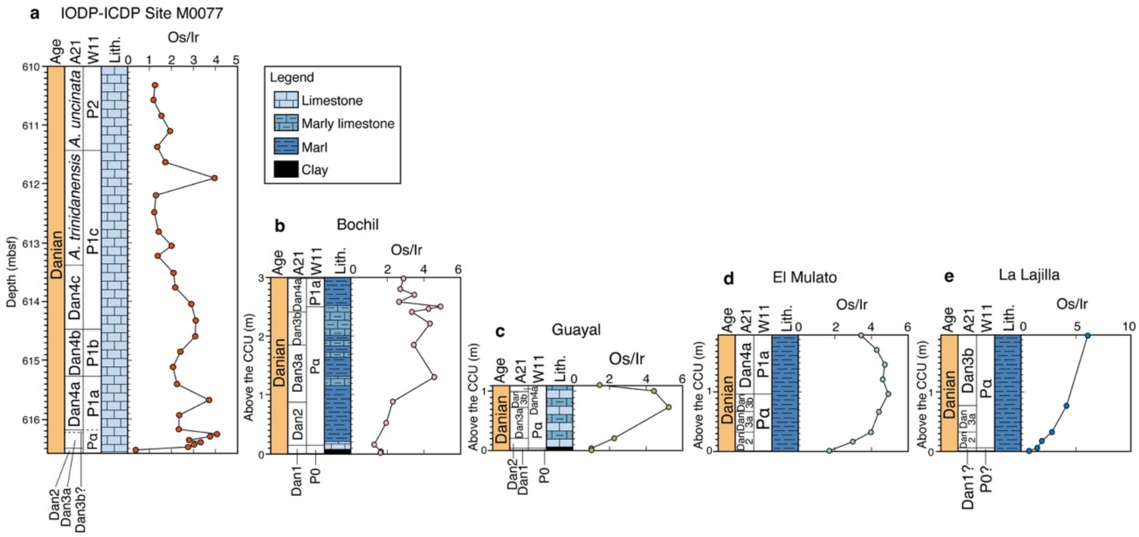

273 **Supplementary Figure 7. Stratigraphic sections showing age, biozones, lithology,**
274 **and Os/Ir ratios in the Gulf of Mexico regions. a,** IODP-ICDP Site M0077 within the
275 Chicxulub impact basin. **b,** Bochil, **c,** Guayal, **d,** El Mulato, and **e,** La Lajilla sections.
276 Planktic foraminiferal zonations A21 and W11 are from Ref.[4] and Ref.[5], respectively.

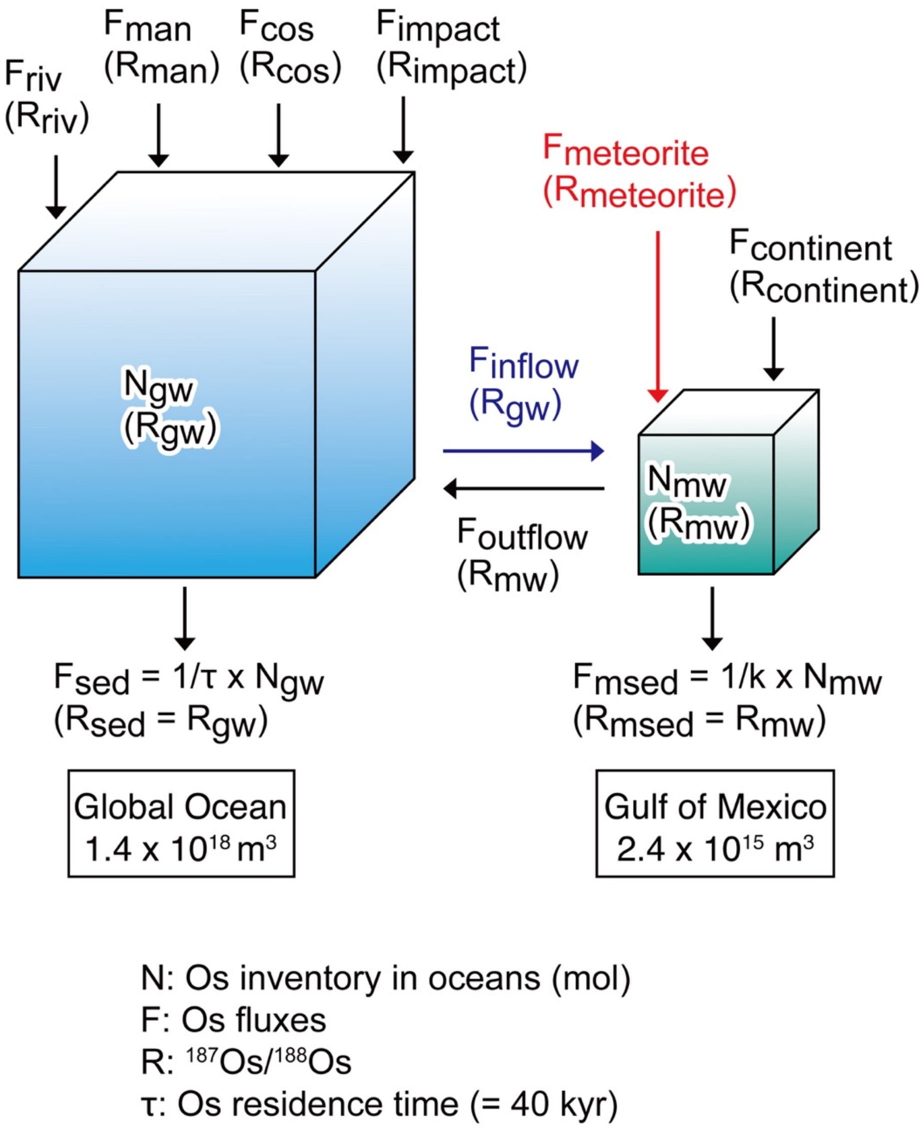

Supplementary Figure 8. Conceptual illustration of the Os mass balance model for global ocean and the Gulf of Mexico after the K/Pg impact. Detailed parameters are given in Supplementary Data 6.

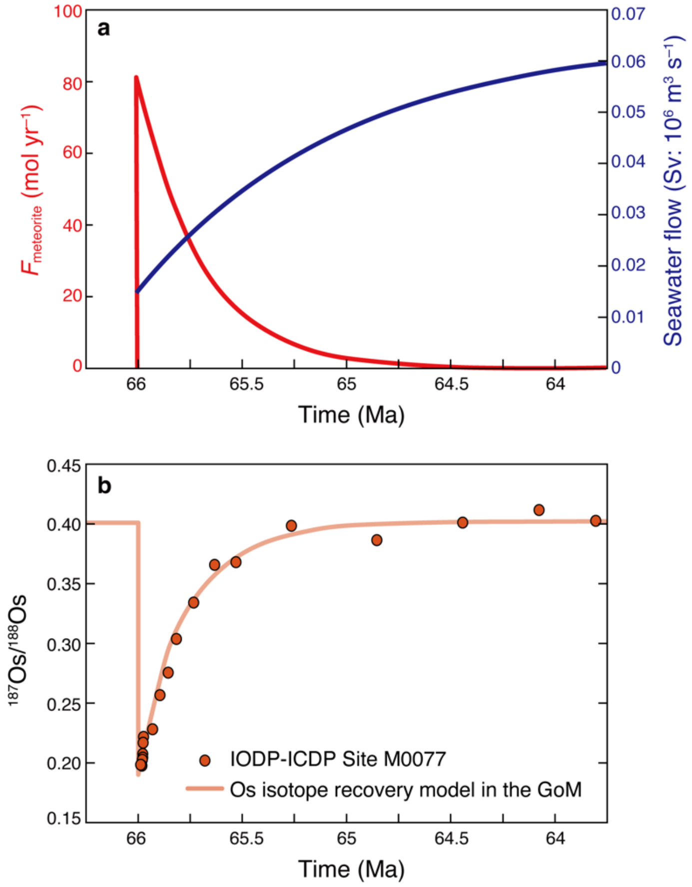

Supplementary Figure 9. Os isotope recovery model in the Gulf of Mexico after the K/Pg impact. a, A diagram contour of Os isotope ratio of the Gulf of Mexico as a function of the influx of unradiogenic Os from the impact ejecta deposit surrounding the Gulf of Mexico or venting of hydrothermal fluids that reacted with the impact melt sheet in the impact basin (red line) and seawater flow through the Gulf of Mexico (blue line). **b,** Modeled $^{187}Os/^{188}Os$ curve in the Gulf of Mexico. The red line represents Os isotope recovery model in the Gulf of Mexico.

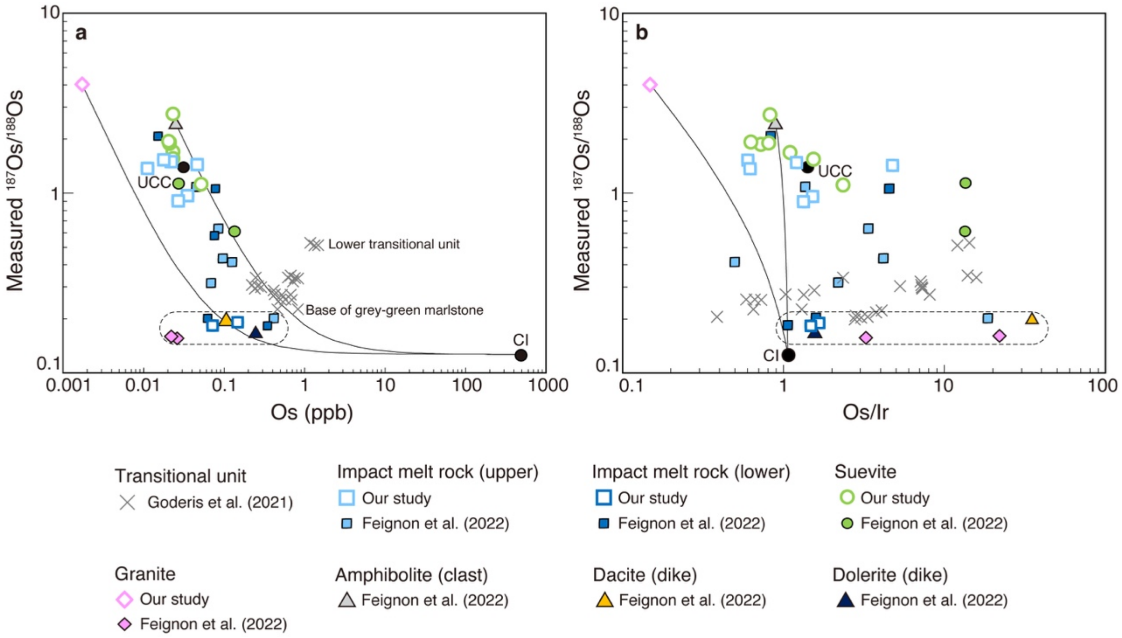

Supplementary Figure 10. Osmium isotope ratios versus Os concentrations and Os/Ir ratios. Measured $^{187}Os/^{188}Os$ ratios versus Os concentrations (**a**) and Os/Ir ratios (**b**) obtained from the transitional unit, suevite, impact melt rocks, and pre-impact lithologies at Site M0077. The curves represent the calculated mixing line between granite-amphibolite and CI chondrite[32]. For comparison, UCC value[33] and the data reported in the previous studies[22,24] are shown in the figure.

Supplementary References

1. Morgan, J. V. et al. *Proceedings of the International Ocean Discovery Program, Volume 364: Drilling the K-Pg impact crater* (International Ocean Discovery Program, College Station, TX, 2017).
2. Grajales-Nishimura, J. M. et al. Chicxulub impact: The origin of reservoir and seal facies in the southeastern Mexico oil fields. *Geology* **28**, 307–310 (2000).
3. Arenillas, I. et al. Chicxulub impact event is Cretaceous/Paleogene boundary in age: New micropaleontological evidence. *Earth Planet. Sci. Lett.* **249**, 241–257 (2006).
4. Arenillas, I., Gilabert, V. & Arz, J. A. New biochronological scales of planktic foraminifera for the early Danian based on high-resolution biostratigraphy. *Geosciences* **11**, 479 (2021).
5. Wade, B. S., Pearson, P. N., Berggren, W. A. & Pälike, H. Review and revision of Cenozoic tropical planktonic foraminiferal biostratigraphy and calibration to the geomagnetic polarity and astronomical time scale. *Earth-Sci. Rev.* **104**, 111–142 (2011).
6. Smit, J. et al. Coarse-grained, clastic sandstone complex at the K/T boundary around the Gulf of Mexico: Deposition by tsunami waves induced by the Chicxulub impact? *Geol. Soc. Am, Spec. Pap.* **307**, 151–182 (1996).
7. Arz, J.A. et al. No evidence of multiple impact scenario across the Cretaceous/Paleogene boundary based on planktic foraminiferal biochronology. *Geol. Soc. Am. Spec. Pap.* **557**, 415–448 (2022).
8. Arenillas, I., Arz, J. A. & Molina, E. A new high-resolution planktic foraminiferal zonation and subzonation for the lower Danian. *Lethaia* **37**, 79–95 (2004).
9. Renne, P. R. et al. Multi-proxy record of the Chicxulub impact at the Cretaceous-Paleogene boundary from Gorgonilla Island, Colombia. *Geology* **46**, 547–550 (2018).
10. Peucker-Ehrenbrink, B. & Ravizza, G. The marine osmium isotope record. *Terra Nova* **12**, 205–219 (2000).
11. van der Ploeg, R. et al. Middle Eocene greenhouse warming facilitated by diminished weathering feedback. *Nat. Commun.* **9**, 2877 (2018).

12. Sato, H. et al. Rhenium-osmium isotope evidence for the onset of volcanism in the central Panthalassa Ocean during the Norian “chaotic carbon episode”. *Glob. Planet. Chang.* **229**, 104239 (2023).
13. Ravizza, G. & VonderHaar, D. A geochemical clock in earliest Paleogene pelagic carbonates based on the impact-induced Os isotope excursion at the Cretaceous-Paleogene boundary. *Paleoceanogr.* **27**, PA3219 (2012).
14. Kuwahara, Y. et al. Rapid coupling between solid earth and ice volume during the Quaternary. *Sci. Rep.* **11**, 5695 (2021).
15. Müller, R. D., Sdrolias, M., Gaina, C. & Roest, W. R. Age, spreading rates, and spreading asymmetry of the world's ocean crust. *Geochem. Geophys. Geosyst.* **9**, Q04006 (2008).
16. Li, G. & Elderfield, H. Evolution of carbon cycle over the past 100 million years. *Geochim. Cosmochim. Acta* **103**, 11–25 (2013).
17. Ravizza, G. & Peucker-Ehrenbrink, B. Chemostratigraphic evidence of Deccan volcanism from the marine osmium isotope record. *Science* **302**, 1392–1395 (2003).
18. Schoene, B. et al. U-Pb constraints on pulsed eruption of the Deccan Traps across the end-Cretaceous mass extinction. *Science* **363**, 862–866 (2019).
19. Paquay, F. S., Ravizza, G. E., Dalai, T. K. & Peucker-Ehrenbrink, B. Determining chondritic impactor size from the marine osmium isotope record. *Science* **320**, 214–218 (2008).
20. Snedden J. W., Lowery C. M. & Lawton T. F. The end of the Cretaceous: depositional palaeogeographical reconstruction of the Gulf of Mexico and adjacent areas just prior to the Chicxulub impact. *Geol. Soc., London, Spec. Pub.* **545**, SP545 (2024).
21. Scott, E., Denne, R., Kaiser, J. & Eickhoff, D. Impact on sedimentation into the north-central deepwater Gulf of Mexico as a result of the Chicxulub event. *Gulf Coast Assoc. Geol. Sci. J.* **3**, 41–50 (2014).
22. Goderis, S. et al. Globally distributed iridium layer preserved within the Chicxulub impact structure. *Sci. Adv.* **7**, eabe3647 (2021).
23. Koeberl, C. et al. Evidence for a meteoritic component in impact melt rock from the Chicxulub structure. *Geochim. Cosmochim. Acta* **58**, 1679–1684 (1994).

24. Feignon, J.-G. et al. Search for a meteoritic component within the impact melt rocks of the Chicxulub impact structure peak ring, Mexico. *Geochim. Cosmochim. Acta* **323**, 74–101 (2022).
25. Mann, P. Gulf of Mexico, Central America, and the Caribbean. In *Encyclopedia of Geology (Second Edition)*, 47–67 (Academic Press, 2021).
26. Lowery, C. M. et al. Rapid recovery of life at ground zero of the end-Cretaceous mass extinction. *Nature* **558**, 288–291 (2018).
27. Lowery, C. M. et al. Early Paleocene paleoceanography and export productivity in the Chicxulub crater. *Paleoceanogr. Paleoclimatol.* **36**, e2021PA004241 (2021).
28. Lowery, C. M. & Bralower, T. J. Elevated Post K-Pg Export Productivity in the Gulf of Mexico and Caribbean. *Paleoceanogr. Paleoclimatol.* **37**, e2021PA004400 (2022).
29. Morgan, J. V. et al. The formation of peak rings in large impact craters. *Science* **354**, 878–882 (2016).
30. Schulte, F. M. et al. Ocean resurge-induced impact melt dynamics on the peak-ring of the Chicxulub impact structure, Mexico. *Int. J. Earth Sci.* **110**, 2619–2636 (2021).
31. de Graaff S. J. et al. New insights into the formation and emplacement of impact melt rocks within the Chicxulub impact structure, following the 2016 IODP-ICDP Expedition 364. *Geol. Soc. Am. Bull.* **134**, 293–315 (2022).
32. Fischer-Gödde, M., Becker, H. & Wombacher, F. Rhodium, gold and other highly siderophile element abundances in chondritic meteorites. *Geochim. Cosmochim. Acta* **74**, 356–379 (2010).
33. Peucker-Ehrenbrink, B. & Jahn, B.-m. Rhenium-osmium isotope systematics and platinum group element concentrations: Loess and the upper continental crust. *Geochem. Geophys. Geosyst.* **2**, 2001GC000172 (2001).
34. Chen, K. et al. Platinum-group element abundances and Re–Os isotopic systematics of the upper continental crust through time: Evidence from glacial diamictites. *Geochim. Cosmochim. Acta* **191**, 1–16 (2016).